CSCE Annual Conference

Growing with youth – Croître avec les jeunes

Laval (Greater Montreal)

June 12 - 15, 2019

EXPERIMENTAL AND ANALYTICAL INVESTIGATION INTO THE EFFECT OF CORROSION ON THE FLEXURAL RESPONSE OF REINFORCED CONCRETE BEAMS

W. Njeem[1,2], A. Vadeboncoeur[1], B. Martín-Pérez[1], A. Jrade[1] and H. Aoude[1]
[1]University of Ottawa, Ottawa ON, Canada
[2]wnjee006@uottawa.ca

Abstract: The aim of this study is to investigate, experimentally and analytically, the effect of reinforcement corrosion on the flexural and shear behaviour of reinforced concrete beams. As part of the experimental study, four beams constructed with normal-strength concrete were tested under four-point bending. Two of the specimens were subjected to an accelerated corrosion process, to reach a target mass loss of 30% and 15% in the longitudinal and transverse steel reinforcement respectively. The other two beams were used as benchmarks with no corrosion. As part of the analytical study the response of the beams was simulated using 2D finite element software (VecTor2) and compared to the experimental results. In addition, a parametric study was conducted using finite element analysis to further examine the effect of other variables such as: level of corrosion (15% vs. 30% mass loss) and the location of the corrosion on the steel reinforcement in the tension zone (full length, mid length and both sides length). The experimental and analytical results show that the increase of mass loss in the steel reinforcement decreases the strength and ductility of the reinforced concrete beams, regardless of the corrosion location, ultimately changing the failure mode. Lastly, the predicted results from the finite element software provide acceptable predictions compared to the experimental results.

1 INTRODUCTION

Reinforcing steel corrosion is considered one of the main deterioration mechanisms of reinforced concrete structures. This phenomenon leads to damage on the protective passive film around the steel bar due to the presence of sufficient quantities of chloride ions and/or carbonation of the concrete cover. In addition to reduction of the reinforcing steel cross-sectional area, the lower-density by-products of the corrosion process exert an expansion on the surrounding concrete, eventually leading to cover cracking (Bicer et al., 2018). Zhang et al. (2019) have indicated that the process of reinforcing steel corrosion is the most influencing factor on the evaluation of durability performance and maintenance of reinforced concrete structures, especially in marine and highway infrastructure exposed to chlorides from seawater or de-icing salts, respectively. Reinforcement corrosion in a reinforced concrete beam reduces the bond between rebars and concrete, which influences the structural performance of flexural elements, such as load-carrying capacity, deformation, ductility, etc. (Hon et al., 2019). Losing the bond between the steel reinforcement and concrete due to corrosion affects the safety and service life of reinforced structures (Li et al, 2018). The corroded steel reinforcement in concrete degrades the bond between concrete and steel bars, reducing the stiffness of reinforced concrete beams and increasing their deflection during their service life (Zhang et al., 2018).

This paper provides the results of an experimental and analytical investigation of the effect of reinforcing steel corrosion on the flexural response of reinforced concrete beams. As a part of the experimental and analytical study, four beams were constructed with normal-strength concrete and tested under four-point bending. Two of the beams were subjected to an accelerated corrosion process to reach 15% and 30% of steel mass loss. All the beams were simulated using 2D finite element software (VecTor2). In addition, a parametric study was conducted using finite element analysis to examine the level of corrosion (15% vs. 30% mass loss) and the location of the corrosion on the steel reinforcement in the tension zone (full length, mid length and both sides length).

2 EXPEREIMENTAL PROGRAM

2.1 Specimen Geometry

A total of four beams were constructed with normal-concrete strength. The first two beams were reinforced with two normal 10M longitudinal bars in the tension and compression zones. The other two beams were reinforced with two normal 25M longitudinal bars in the tension zone and 2-10M longitudinal bars in the compression zone. Transverse reinforcement consisted of U-shaped stirrups made from 6.3-mm wires spaced at 100 mm throughout the full length of the specimen for all beams. Two beams, one with 10M and the other with 25M tensile reinforcement were subjected to an accelerated corrosion process to achieve a targeted steel mass loss of 30% and 15% in the longitudinal and transverse steel reinforcement, respectively (beams **BMC30** and **BSC15**). The remaining two beams with 10M and 25M tensile reinforcement were used as benchmarks with no corrosion (controls: **BF0** and **BS0**).

As shown in **Figure 1**, the beams had dimensions of 125 mm x 250 mm x 2440 mm and were tested over a simply-supported span of 2,232 mm. **Table 1** shows a summary of the design of the four beams and provides information on concrete and longitudinal reinforcement properties as well as the location of the corrosion and corrosion level.

Table 1. Specimens designation and main properties

#	Beam ID	Concrete	Longitudinal Reinforcement		Stirrups	Corrosion Location	Mass Loss %
		f'_c (MPa)	Top	Bottom	Size (mm)		
1	BF0	35	2-10M	2-10M	6.3	-	0
2	BMC30	47	2-10M	2-10M	6.3	10M bars-Mid length (750 mm)	30
3	BS0	46	2-10M	2-25M	6.3	-	0
4	BSC15	43	2-10M	2-25M	6.3	6.3 stirrups-Shear	15

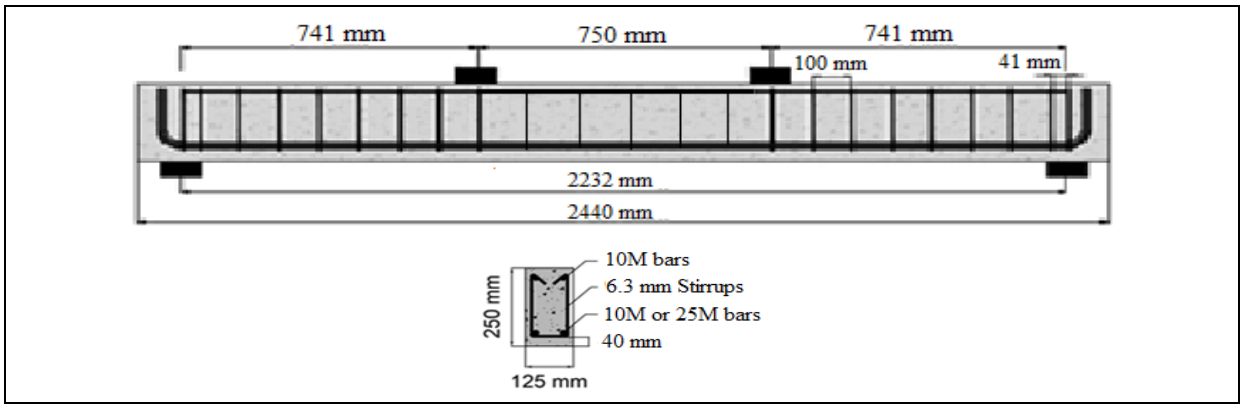

Figure 1. Beams dimensions and details of reinforcement

2.2 Materials

The concrete mix design of this investigation consisted of water, GU cement, fine aggregate, coarse aggregate and 3% salt (NaCl) of the cement weight. The quantities of the mix components are listed in **Table 2**. The compression strength of the concrete used in each reinforced concrete beam was tested using a cylinder with dimensions of 100 mm x 200 mm and is listed in **Table 1**. In addition, **Figure 2** illustrates the stress-strain curves for concrete and the longitudinal and transverse steel reinforcement (10M & 6.3 mm bars, respectively).

2.3 Corrosion Acceleration Process

In this investigation the corrosion was accelerated using an impressed current technique. The procedure of this technique starts by placing the beams in a tank filled with normal tap water. The depth level of water in the tank was around 110 mm. Wet sponges were placed on the top of each beam, and stainless steel plates acting as cathodes were placed on top of the wet sponges at the location of intended corrosion. Either the longitudinal tensile reinforcement (specimen **BMC30**) or the stirrups (specimen **BSC15**) were corroded and therefore acted as anodes. All the beams were connected to a power supply to reach the desirable mass loss of 15% and 30% as illustrated in **Figure 3**.

Table 2. Concrete mix components

Mix components	**Quantities**
Water	199 kg/m^3
GU Cement	410 kg/m^3
Coarse aggregate	1099 kg/m^3
Fine aggregate	609 kg/m^3
Salt	12.3 kg/m^3

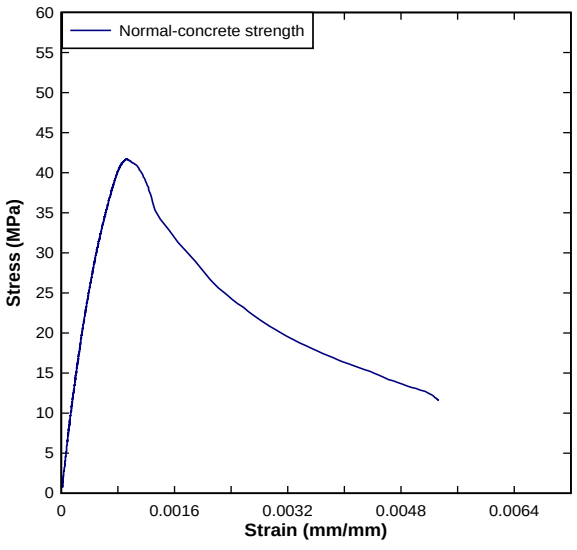

a).Concrete (compression)

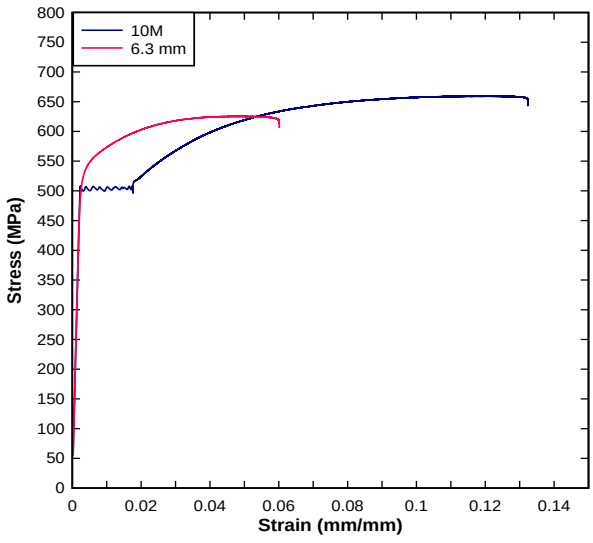

b). Steel reinforcement

Figure 2. Material stress-strain relationships

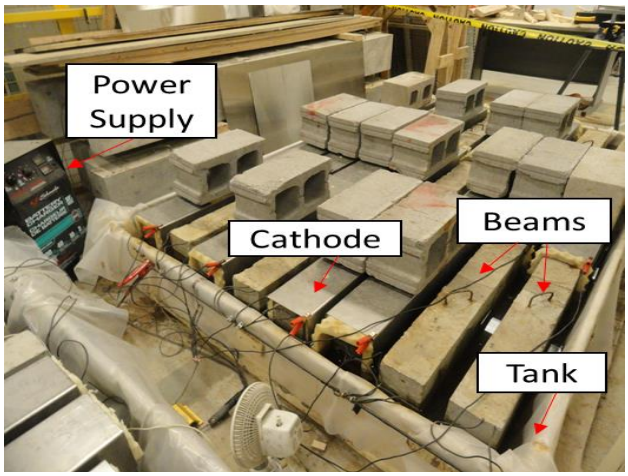

a). Corrosion setup components

b). Typical beam after corrosion

Figure 3. Corrosion set up

2.4 Test Setup

The setup shown in **Figure 4** was used to test all beams under quasi-static four-point bending. The beams were simply supported over a span of 2232 mm, with a constant moment region of 750 mm and two equal shear-spans of 741 mm. A manually operated hydraulic jack was used to apply the loading which was then transferred to the specimens as two point loads using a steel spreader beam. The load was recorded using a load-cell placed below the hydraulic jack, with displacement at mid-span captured using a cable displacement transducer. Strains in the reinforcing bars were monitored using strain-gages which were applied on the tension steel at mid-span. Loading of the beams began under load-control until signs of yielding were detected. Upon yielding, loading continued under displacement-control until failure of the specimens (concrete crushing or shear collapse).

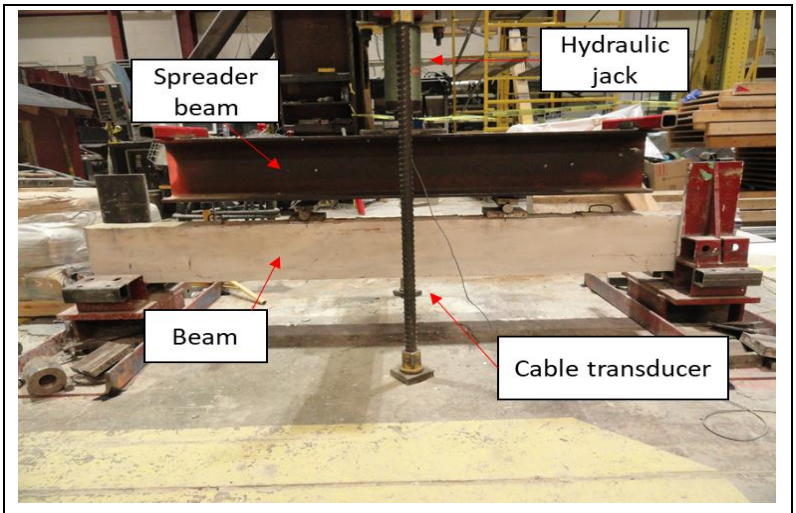

Figure 4. Test setup

3 EXPEREIMENTAL RESULTS

The load-deflection response of the 10M and 25M series are plotted in **Figure 5(a)** and **Figure 5(b)**, respectively. **Table 3** summarizes key data extracted from the load-deflection curves, including yield load (P_y) and maximum load (P_{max}), yield displacement (Δ_y) and maximum (failure) displacement (Δ_{max}), beam stiffness (T) after cracking, ductility (Δ_{max}/Δ_y) and toughness (A_u), taken as the area under the load-deflection curve until Δ_{max}. The failure displacement corresponding to 85% of P_{max} (Δ_{85}) is also reported.

Figure 5 (a) shows that the yield strength of beam **BF0** was 54 kN at a deflection of 11 mm, the maximum capacity reached 61 kN and the maximum displacement recorded was 120 mm. The failure displacement (Δ_{85}), stiffness, ductility and toughness reached 90 mm, 4,837 N/mm, 11 and 6,525 kN-mm respectively. In addition, this beam experienced a ductile flexural failure mode with significant yielding of the longitudinal bars prior to crushing the concrete in the compression zone. The resulting cracking pattern, typical of flexural failure, is illustrated in **Figure 6 (a)**. Beam **BMC30** experienced lower yield and maximum strengths than beam **BF0** due to the effect of corrosion with reductions of 8.9% and 13.8% for (P_y and P_{max}) respectively. The failure and maximum displacements, stiffness, ductility and toughness of this beam were also lower than **BF0,** as shown in **Figure 5 (a)** and **Table 3** with reductions of 60%, 40.8%, 9.7%, 45.4% and 29.4% in (Pmax (Δ_{85}), $\Delta_{max,}$ T, Δ_{max}/Δ_y and A_u) respectively. Furthermore, the failure mode was affected by the steel corrosion with the beam failing suddenly due to rupture of the reinforcement in the tension zone, and the resulting cracking pattern is illustrated in **Figure 6 (b)**.

Figure 5 (b) illustrates the load-deflection response of the beams in the second set which examined the effect of corrosion in the transverse steel. As shown in this figure and **Table 3**, the maximum strength of beam **BS0** reached 190 kN. In addition, the maximum displacement, failure displacement (Δ_{85}) and the toughness recorded were 84 mm, 25 mm and 8635 kN-mm, respectively. This beam experienced a sudden shear failure before yielding of the longitudinal reinforcement and prior to crushing of the concrete in the compression zone. Failure was associated with a diagonal shear crack in the right shear-span region, with buckling of the longitudinal bars in between the stirrups in the compression zone, as shown in **Figure 6 (c)**. **Figure 5 (b)** shows that the maximum strength of beam **BSC15** reached 198 kN, which is slightly higher than beam **BS0**; however, the post-peak response as affected with lower failure displacement (Δ_{85}), maximum displacement and toughness when compared to beam **BS0** due to the influence of corrosion in the stirrups, with reductions of 16%, 23.8% and 30.5% in these parameters as presented in **Table 3**. The failure mode of beam **BSC15** was in shear with significant buckling of the longitudinal bars in the compression zone in the right side shear-span region. As shown **Figure 6 (d)** the damage and cracking was more significant with loss of the side concrete cover at failure.

Table 3: Experimental results extracted from load-deflection curves

Beam I.D.	Load		Displacement			Stiffness (N/mm)	Ductility Δ_{max}/Δ_y	Toughness A_u (kN-mm)
	Yield P_y (kN)	Max. P_{max} (kN)	Yield Δ_y (mm)	Δ_{85} (mm)	Failure Δ_{max} (mm)			
BF0	54	61	11	90	120	4837	11	6525
BMC30	49	53	11	36	71	4367	6	4605
BS0	-	190	-	25	84	-	-	8635
BSC15	-	198	-	21	64	-	-	6000

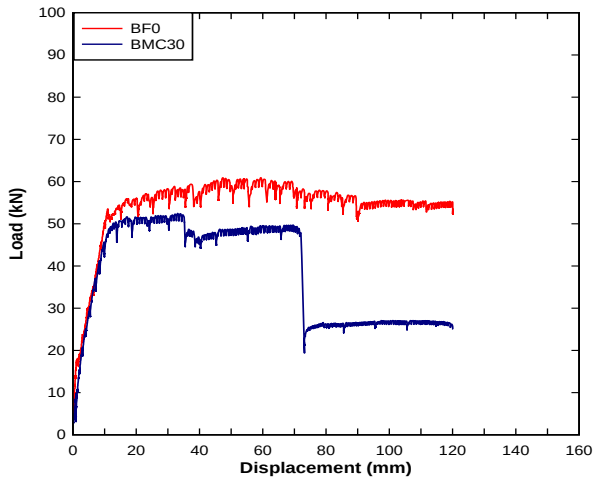

a) 10M series

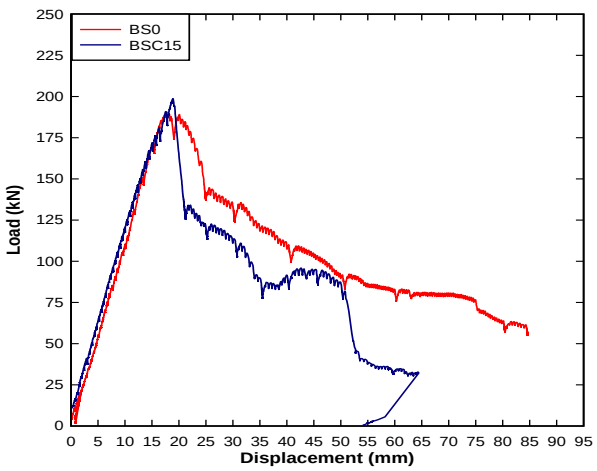

b) 25M series

Figure 5. Load-deflection curves

a).(BF0)

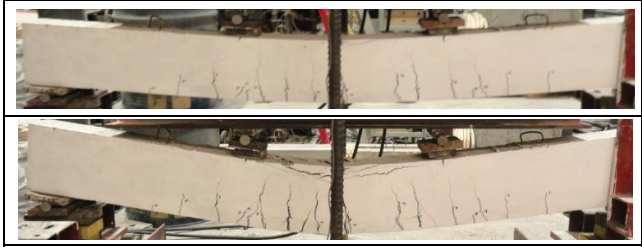

c).(BS0)

b).(BMC30)

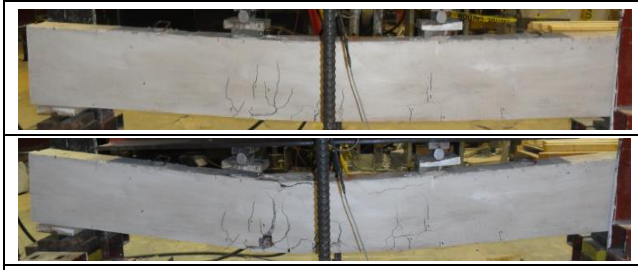

d).(BSC15)

Figure 6. Failure mode for all beams

4 FINITE ELEMENT ANALYSIS

4.1 Analytical Methodology

2D nonlinear finite element software (VecTor2) was used to predict the flexural response of the uncorroded and corroded reinforced concrete beams tested in this study (Section 4.1). In addition, the effect of corrosion location on the tensile reinforcement (mid length) and transverse reinforcement was also investigated as discussed in (Section 4.2).

Half of the simply-supported beam was modelled in VecTor2 as shown in **Figure 7**. The pre-peak and post-peak response of the concrete in compression was modelled using the Popovics (NSC) and Popovics / Mander models, respectively, with the maximum crack width fixed at 10 mm. The concrete element type in the model consisted of 4-node rectangular plane-stress element with 2 degrees of freedom, and the mesh size was 10 mm x 10 mm. The reinforcement was modeled using a trilinear elastic-hardening curve. Concrete properties (tensile strength, modulus and concrete peak strain) were calculated according to the equations provided in the VecTor2 manual, except the compression strength which was determined from the experimental tests. The steel reinforcement properties were also provided based on the experimental results. The longitudinal steel reinforcement was modelled as truss elements, and the transverse reinforcement was also simulated as discrete truss elements or smeared in the concrete elements. The corrosion process was considered by reducing the cross-sectional area of the steel bars based on the mass loss and by applying a pre-strain of -30 mε on the concrete elements surrounding the steel bar that was corroded to simulate induced-cracking (Bernard and Martin-Perez, 2013). The plates at the supports and under the load points were constrained to distribute the stress across the mesh nodes. In addition, displacement was applied on the loading point. The steel bars were assumed to be perfectly bonded to the concrete. A total of 51 and 101 monotonic load stages were applied to the 10M and 25M specimens, respectively.

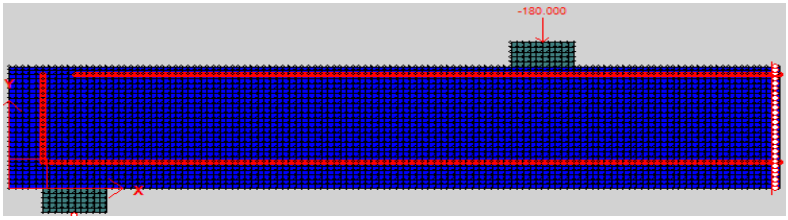

Figure 7. Typical finite element mesh

4.2 Analytical Results

The analytical load-deflection response of the 10M and 25M series beams are plotted in **Figure 8(a)** and **Figure 8(b)**, respectively**. Figure 8 (a)** shows the finite element results of beam **BF0**, with a yield strength of 53 kN at a yield displacement of 7 mm, and a maximum strength of 65 kN at a displacement of 155 mm. The failure mode of this beam is a ductile flexural mode, and the cracking pattern corresponds to that of flexural failure as shown in **Figure 9 (a)**. The analysis of beam **BMC30** led to a yield strength of 42 kN at a displacement of 8 mm and a maximum capacity of 53 kN at a displacement of 141 mm. The yield and maximum strengths in the simulation were lower than those of beam **BF0** as a result of the corrosion of the longitudinal tensile reinforcement. The failure mechanism of the beam was rebar rupture of the longitudinal reinforcement in the tension zone as shown in **Figure 9 (b)**. The stiffness of beams **BF0** and **BMC30** was almost the same, as shown in **Figure 8(a)**. On the other hand, the maximum strength capacity of **BS0** reached 205 kN at a displacement of 13 mm and the maximum displacement recorded in the analysis was 61 mm, while beam **BSC15** recorded a maximum strength of 201 kN at a displacement of 13 mm and the maximum displacement calculated was 80 mm, as presented in **Figure 8 (b).** The failure mechanism was shear failure for both beams (**BS0** and **BSC15**) as illustrated in **Figure 9 (c)** and **(d)**.

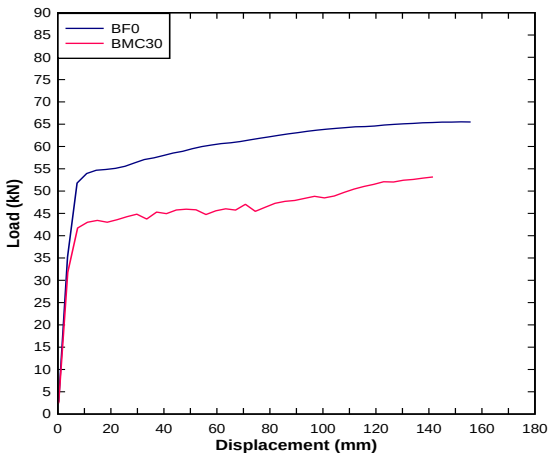

a).10M series

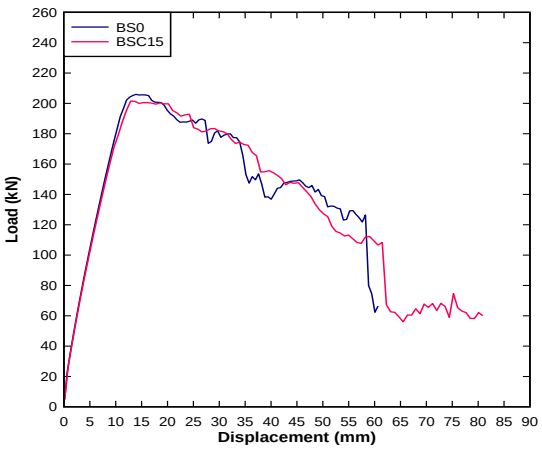

b).25M series

Figure 8. Load-deflection from finite element analysis

a).BF0

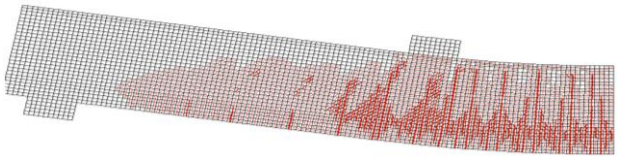

c).BS0

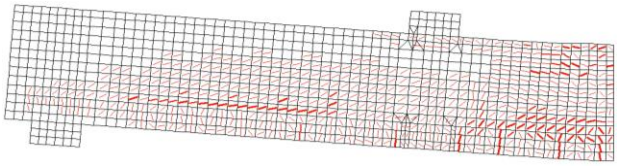

c).BMC30

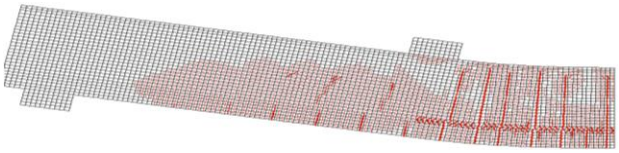

d).BSC15

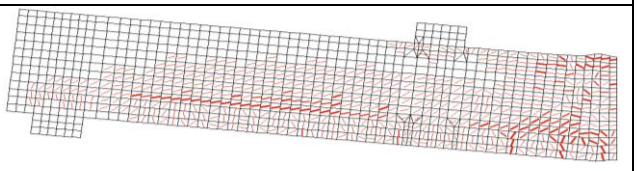

Figure 9. Cracking at failure mode

5 COMPARISON BETWEEN EXPEREIMENTAL AND ANALYTICAL RESULTS

The comparison between experimental and analytical results is presented in **Figure 10**. For beam **BF0**, the predicted results of the simulated beam were acceptable in terms of yield strength, maximum strength, ductility and stiffness when compared with the experimental results (see **Figure 10 (a)**). The yield strength and maximum strength of the simulated beam **BMC30** were lower than the experiment; however, the stiffness was acceptable as shown in **Figure 10 (a)**. As illustrated in **Figure 10 (b)**, the predicted results of simulated beams in the second set (**BS0** and **BSC15**) were acceptable in terms of the maximum strength; however, the stiffness of the simulated beams was higher than the experimental ones, since the bond between the concrete and tensile steel reinforcement was assumed to be perfect while this parameter in the reinforcing bars may have been affected in the experimental beams due to the corrosion process.

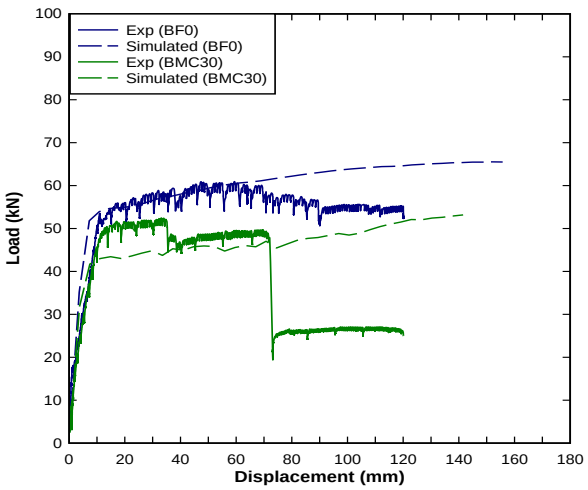

a).10M series

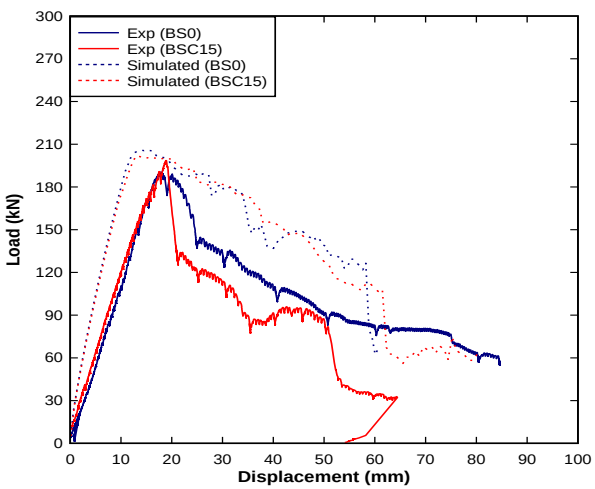

b).25M series

Figure 10. Comparison between experimental and analytical results

6 PARAMETRIC STUDY

Finite element analysis was used to further examine the effect of other variables, such as: - the level of corrosion (15% vs. 30% mass loss) and the location of the corrosion on the tensile steel reinforcement (full length, mid length (750 mm) and both sides length (1,482 mm)). The load-deformation responses obtained from the finite element analysis are illustrated in **Figure 11**. According to the figure, corroded beams with 15% mass loss along the tensile reinforcement had better performance in terms of strength capacity and ductility when compared with beams with 30% mass loss on the tensile bars. Furthermore, the location of corrosion on the steel reinforcement in the tension zone also had influence on the flexural response of the reinforced concrete beams. The beam with corrosion at both sides had good performance in terms of strength capacity and ductility when compared to corroded beams in the middle and full lengths on the tensile reinforcement as presented in **Figure 11**. However, note that the loss of bond at anchorages was not modelled for the analysis with corrosion located at the ends.

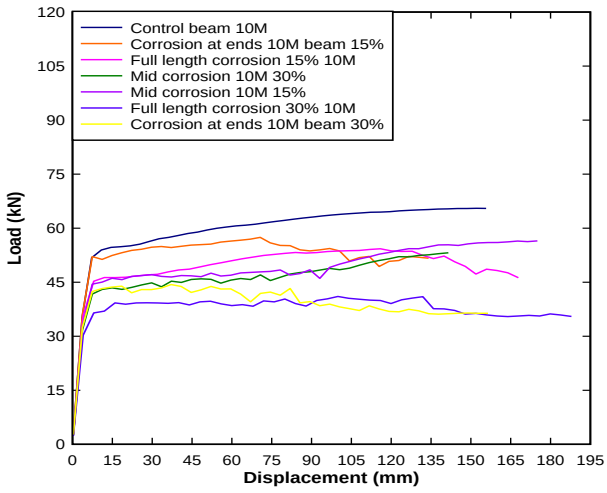

Figure 11. Parametric study

7 CONCLUSION

The results of this investigation examined the effect of steel reinforcement corrosion on the flexural and shear response of reinforced concrete beams. The results show that corrosion of the steel reinforcement in the mid-span tension zone reduces the strength, stiffness, ductility and toughness of the reinforced concrete beams. In addition, it affected the failure mode, with failure occurring due to rupture of the tension steel bars. The analysis shows that the response is more greatly affected as the percentage of mass loss is increased. Furthermore, the location of corrosion on the steel reinforcement in the tension zone (middle length, both sides length and full length) was shown to affect the beam response characteristics. Similarly, the tests show that corrosion in the shear reinforcement had an effect on the post-peak response, cracking pattern and level of damage, although the ultimate shear capacity was not affected. In general, the finite element simulations resulted in acceptable predictions when compared to the experimental results.

8 REFERENCES

Bernard, S. and Martín-Pérez, B. . 2013. Finite Element Modelling of Reinforced Concrete Beams with Corroded Shear reinforcement. CSCE 2013 General Conference.

Bicer, K., Yalciner, H., Balkıs, A. B. and Kumbasaroglu, A. . 2018. Effect of Corrosion on Flexural Strength of Reinforced Concrete Beams with polypropylene fibers. Journal of Construction and Building Materials, 185, 574-588.

Hou, L., Zhou, B., Guo, S., Aslani, F. and Chen, D. . 2019. Corrosion Behaviour and Flexural Performance of Reinforced Concrete/ Ultrahigh Toughness cementitious Composite (RC/UHTCC) Beams Under Sustained Loading and Shrinkage Cracking. Journal of Construction and Building Materials, 198, 278-287.

Li, H., Li, B., Jin, R., Li, S. and Yu, J. G. . 2018. Effects of sustained Loading and Corrosion on the Performance of Reinforced Concrete beams. Journal of Construction and Building Materials, 169, 179-187.

Zhang, H., Wu, J., Jin, F. and Zhang, C. . 2019. Effect of Corroded Stirrups on shear Behaviour of Reinforced Recycled Aggregate Concrete Beams strengthened with Carbon Fiber-Reinforced Polymer. Journal of Composites Part B, 161, 357-368.

Zhang, W., Zhang, H., Gu, X. and Liu, W. . 2018. Structural Behaviour of Corroded Concrete Beams Under Sustained Loading. Journal of Construction and Building Materials, 174, 675-683.